Proceedings of the ASME 2016 Dynamic Systems and Control Conference
DSCC2016
October 12-14, 2016, Minneapolis, Minnesota, USA

DSCC2016-9914

FORCE ANALYSIS AND MODELLING OF SOFT ACTUATORS FOR CATHETER ROBOTS

Mark Gilbertson, Darrin Beekman, Biswaranjan Mohanty, Saeed Hashemi, Sangyoon Lee,
James D Van de Ven, Timothy M Kowalewski
Department of Mechanical Engineering
University of Minnesota
111 Church Street SE, Minneapolis, MN 55455
Email: gilbe767@umn.edu

ABSTRACT

Soft robotic actuators may provide the means to develop a soft robotic catheter, enabling safer and more effective transcatheter procedures. In many clinical applications, device contact force affects the quality of diagnostic or the degree of therapy delivered. Therefore precise end effector force control will be a requirement for the soft robotic catheter. In this study a bending soft actuator system was fabricated, and the relationship between volume input and end effector contact force is examined. Static and dynamic system identification were conducted under two different loading conditions loosely related to actuation in a blood vessel. The experimental data from these tests led to the creation of a non-linear system model. A reduced term model was developed using a Root Mean Square Error (RMSE) method in order to observe the importance of system dynamics and nonlinearities. A different system model was designed for each loading condition. These two reduced models matched with experimental result, but differed in model terms and parameters, suggesting that either loading condition identification or end effector closed-loop sensing will be needed for accurate contact force control of a soft robotic actuator in an intravascular environment.

INTRODUCTION

Endovascular surgery provides many of the benefits of minimally invasive surgery, but the constraints imposed on the surgeon increase time and risk in the catheter lab. Despite the additional technical difficulty, the improved patient outcomes have led to large-scale adoption of transcatheter procedures nationwide. According to the Centers for Disease Control, in 2010, over 4.4 million transcatheter procedures were performed in the United States [1]. Transcatheter procedures, such as balloon angioplasty, transcatheter valve repair, and radiofrequency ablation, enable the physician to provide lifesaving therapies without the trauma induced by conventional surgeries. But because of the remote location of the surgeons control, the imaging limitations inside the vasculature, and the complexity of the anatomy and techniques used, these procedures often increase the time spent in the operating room as well as the degree of difficulty of the procedure [2]. Beyond navigating through the complex vasculature, many of these procedures, whether they are diagnostic or therapeutic, require some element of catheter contact force. Additionally, the degree of contact force can affect the sensing ability of the diagnostic procedure or the even the efficacy of the therapy delivery [3], [4], [5], [6]. Therefore a more optimal form of transvascular navigation and procedure control is needed. This improved method must enable clinicians to easily maneuver throughout complex vasculature, exert specific forces for diagnostic or therapeutic delivery, and maintain specific positions while resisting pulsatile flow in vessels.

In the field of laparoscopic medicine, medical robots have provided a level of tool stability and control unparalleled by conventional laparoscopic methods [7]. Beyond medical applications, robots are often utilized for their precision, speed, and

ability to function in harsh environments. While these benefits are desirable, conventional robotic systems with non-compliant links cannot be utilized intravascularly, as the robot links could easily tear through the fragile vasculature.

Soft robotics may provide the hybrid solution that combines the precision control of traditional robotics with the compliance of transvascular catheters to enable robotic-controlled, transcatheter procedures. Soft actuator kinematic system modeling and identification, electro-hydraulic circuit design, and the eventual control of this system are important to the ultimate design of an effective transvascular catheter robot.

Soft actuators are systems built from compliant and extensible materials. Fluid power is used to expand the compliant cavities of the soft actuator, and strategic application of inelastic strain limiting fibers surrounding the cavity leads to the desired deformation. Initial soft actuator research produced an elastomeric tube with equal and opposite fiber wrapping allowing it to either expand or contract as an internal pressure is applied [8]. Several kinematic and dynamic models have been created which map input pressure to output force for this early soft actuator [9], [10]. Recent research has explored the application of various wrap angles to produce more complex deformations such as twisting, bending, spiral, and screw motion [11]. These actuators are known as fiber-reinforced enclosed elastomers (FREEs) [12], [13], [14], [15], and in addition to kinematic models, axial force and applied moment models have also been developed. [16], [17]. The bender actuator, which is a FREE actuator, has been subject to many modeling endeavors. This low deformation soft actuator has been described as an "elastomeric bladder wrapped with strain-limiting reinforcement" [18], and is comprised of a semi-circular tube that is fiber wrapped and has a strain limiting layer on it flat side [19]. Its simple strain-limiting layer configuration, ease of manufacture, and planar motion has led to several kinematic investigations [20], such as mapping bend angle as a function of input pressure with varying degrees of accuracy [20], [21]. While these kinematic models have advanced soft actuator locomotion systems, more research is needed for transcatheter clinical relevancy. Whether it is transcatheter valve replacement, atrial septal defect closure, atrial fibrillation ablation, intravascular ultrasound, excimer laser angioplasty or novel intravascular tissue sensing modalities [22], [23], most therapies or diagnostics performed intravascularly are sensitive to the degree of device contact force. Inadequate or unstable contact forces can result in sensing errors or insufficient therapy delivery [3], [4], [5], [6]. Beyond the kinematic modeling, however, little work has been done to characterize and model distal tip force output in a clinically relevant environment. Sun et al. were able to characterize the distal tip force of a specific soft bender actuator at a variety of unconstrained bending angles, though no model was produced. Recently, Polygerinos et al. proposed a model to map input pressure to distal tip output force for a soft bender actuator [20]. However this model is only valid for a bending angle of zero degrees, when the actuator is fully constrained so it cannot bend. An output force model still needs to be established for more clinically relevant loading conditions.

Additionally, due to biocompatibility concerns, traditional pneumatic pressurization of soft actuators must be discarded. Any leak of air into the blood stream can result in an air embolism, leading to severe adverse events [24]. Therefore, it is imperative that the soft actuators be driven by a biocompatible fluid like water or saline to maintain clinical relevance. These fluids are already used in the catheter lab to inflate angioplasty balloons during surgical procedures and their low compressibility allows for easier volume control. Scaling these hydraulic sources down to the forces required for miniature actuation, however, can cause dynamic performance issues from frictional forces and gravity effects, which will complicate any model [25].

When applied to transvascular surgery, soft actuators have an opportunity to reduce adverse events, reduce healthcare costs, and improve clinical outcomes by combining the precision, control, and speed of robots with the safety and compliance of intravascular catheters. Contact force control of these actuators is an important element of the future soft catheter robot design, as many transcatheter diagnostics and therapies are sensitive to the degree of device contact force. In this study, a soft bender actuator is hydraulically powered via water instead of clinically incompatible pneumatic power, and a new force model is proposed and empirically evaluated. This model relates input volume to output force at the end effector under two clinically motivated loading conditions.

METHODS

Soft Robot Design and Fabrication

The soft robotic bending actuator was designed and fabricated using the methods listed in the Soft Robotic Toolkit [26]. The semicircular bending actuator is capable of providing higher bending force than a circular cross section at a given pressure, which provides more efficient force transmission at the tip. The main body of the bender was made from an addition cure silicone rubber (Dragon Skin® 00-30A, Smooth-On Inc.). This silicone was poured into a custom mold made from a 3D printer (Replicator 5th Generation, MakerBot LLC) in combination with a half round aluminum rod cut to size. The mold also included groove feature indentations along the circumferential surface to hold the radial strain limiting layer. Once the silicone body of the bender actuator had cured, strain limiting layers were added. A ribbon (Berwick Offray LLC) was used as the axial strain limiting layer and adhered to the flat surface of the bender with silicone rubber adhesive (Sil-Poxy®, Smooth-On Inc.). The radial strain limiting layer was created by wrapping fishing line (20-lb Berkley® FireLine®, Pure Fishing, Inc.) in the grooves of the bender. This formed two equally opposing helices with a mesh density to prevent bulging. To create a seal, one end of the bender was dip

molded and the other attached to a standard National Pipe Thread barbed fitting. The soft bender actuator is shown in Figure 1 and the dimensions of the actuator are listed in Table 1. These dimension were chosen to aid prototype development.

TABLE 1: Dimensions of Soft Bender Actuator

Inner Diameter	Wall Thickness	Length	Wrap Angle
12.7*mm*	2*mm*	170*mm*	$\pm 80°$

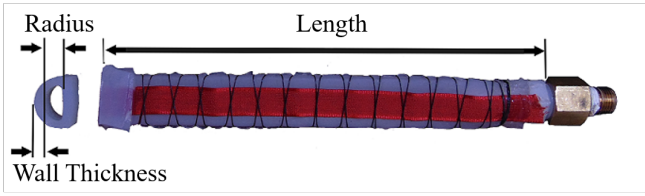

FIGURE 1: Soft actuator with labeled dimensions

Electro-Hydraulic System and Test Setup

Electro-Hydraulic System Using water as the hydraulic fluid, a hybrid hydraulic and electrical system was built to drive the soft actuator. The electro-hydraulic circuit was comprised of a linear actuator (4-in, 25-lb Thrust Linear Actuator ServoCity, Robotzone, LLC) connected to a hydraulic cylinder (1-1/16" cylinder - 2" stroke, Bimba Manufacturing Company). The linear actuator was controlled via a motor driver chip (TBG549PG, Toshiba) connected to an Arduino microprocessor (Arduino Nano, Arduino LLC). By controlling the linear actuator, and subsequently the position of the hydraulic piston, the volume within the bender actuator could be modulated. A linear variable differential transformer, (LVDT) (LD630-100, OMEGA Engineering Inc.) was attached to the linear actuator in order to precisely measure the position of the cylinder piston which was used to calculate volume flow into the bender. A pressure transducer (MLH100PGL06A, Honeywell International Inc.) was connected at the distal end of the hydraulic circuit, just above the bender actuator, in order to monitor the pressure within the soft robotic segment. The electro-hydraulic experimental setup can be seen in Figure 2.

Test Apparatus A test apparatus was assembled in order to provide: (1) a solid base upon which to mount the bender and

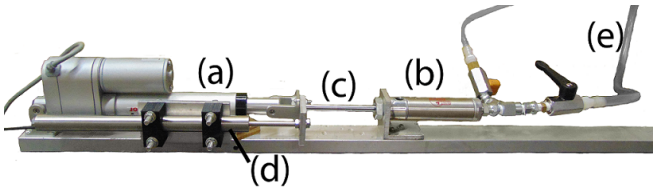

FIGURE 2: Electro-hydraulic circuit: (a) linear actuator, (b) stroke cylinder, (c) cylinder piston rod, (d) a LVDT, and (e) tubing leading to the bender.

(2) an environment in which to measure the force applied by the bender in the appropriate loading configurations.

The test frame and base functionality of the test apparatus was built from a modified 3D printer (CubeX, 3D Systems, Inc). A custom aluminum adapter enabled the bender to mount to the carriage of the 3D printer. In order to measure the force applied by the distal tip of the bender, a load cell (3132, Phidgets Inc.) connected to a 24-bit analog to digital converter (AD7730, Analog Devices) was mounted to the tray of the modified 3D printer. The test apparatus can be seen in Figure 3, including the test frame, the load cell, and the bender actuator.

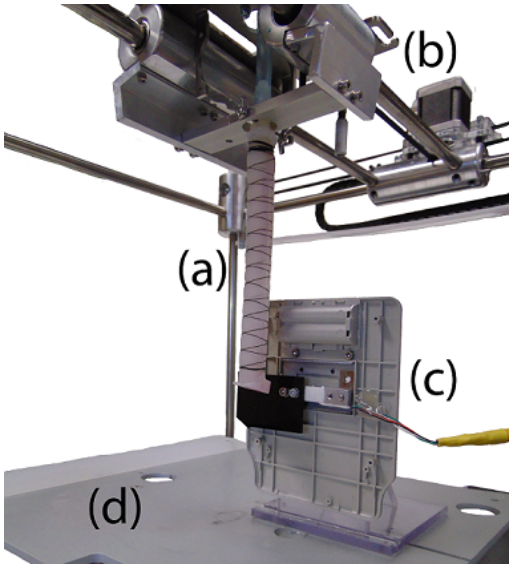

FIGURE 3: The test apparatus comprising (a) the soft robotic bender actuator, (b) the gantry carriage of a modified 3D printer, (c) the load cell to measure the contact force of the bender, and (d) the modified 3D printer tray.

The contact force applied by the bender actuator was measured under two different loading conditions as shown in Figure 4. These two loading conditions were selected to mimic the en-

vironment a soft robotic catheter might encounter in the vasculature.

The unconstrained configuration allows the bender arch to stretch laterally when reacting to the force experienced at the distal tip. An example of this condition in the anatomy is the bender operating in larger vasculature or even a chamber of the heart such that the distal tip contacts one side of the anatomy wall without the bender body arch contacting the opposite wall. For applications in a more constricting vascular environment, the constrained configuration adds a roller joint halfway up the length of the actuator to simulate the bender arch contacting the opposite side of the vascular wall.

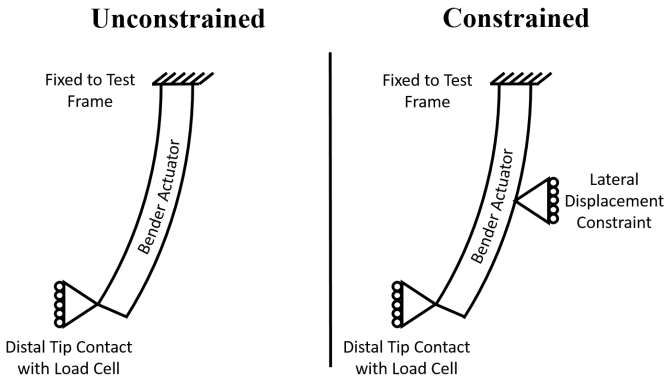

FIGURE 4: Unconstrained and constrained loading conditions.

System Identification and Characterization

To identify a system model that maps input volume to output force at the distal tip of the soft actuator, two open loop evaluations were performed: (1) the static system response test and (2) the dynamic system response test.

In these tests, a pulse-width modulated (PWM) voltage was sent to the electro-hydraulic linear actuator to control the volume of the soft actuator. The LVDT recorded the piston displacement which was used to derive a volume measurement. The pressure and force at the distal tip of the soft actuator were recorded via the pressure transducer and load cell respectively, at a rate of $83Hz$.

Static System Response The static response was characterized by two tests: a ramp and staircase response. The single level quasi-static ramp analysis was performed in order to understand the one-to-one relationship between force and input volume. The amplitude of PWM voltage was increased by $47mV$ every $8s$, as shown in Figure 5(a), until a pressure of $101.3kPa$ had been reached in the soft actuator.

A multi-level staircase loading and unloading test was performed to understand the hysteresis in the force output due to time fatigue in the material. Alternating step signals were sent to the linear actuator which increased in amplitude by $47mV$ with every cycle. Each cycle had a period of $15s$. The first $12s$ of the cycle increased the volume of the soft actuator at a specified rate. The final $3s$ of the cycle retracted the cylinder at full power, draining the volume. A sample of the multi-level square signal is depicted in Figure 5(b).

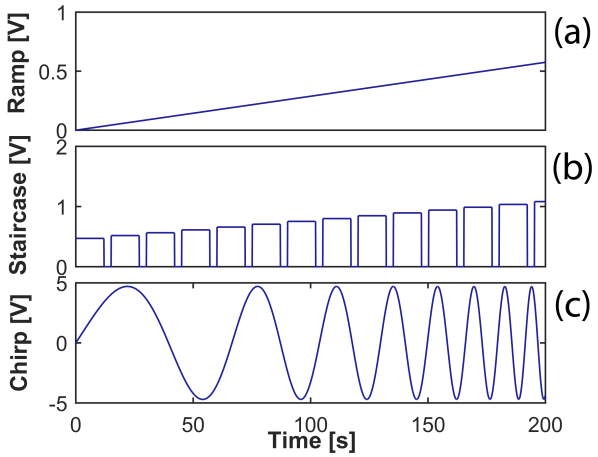

FIGURE 5: Test signals used for characterizing both static response with quasi-static ramp (top), and multi-level staircase (middle), and the dynamic response via a chirp response (bottom).

Dynamic System Response To measure the dynamic response of the system, a frequency sweep was performed. A chirp signal ranged from $f_i = 0.01Hz$ to $f_f = 5Hz$ was chosen based on the bandwidth of the bender as well as limitations in the electro-hydraulic circuit. This signal has a rate of L, where t_f was the final time of $1800s$. The signal had an amplitude of $a = 4.71V$ as shown in Figure 5(c) derived from [27] and reproduced in Eqn. (1) and Eqn. (2).

$$s(t) = a \sin 2\pi f_i L[\exp(t/L) - 1] \tag{1}$$

$$L = \frac{t_f}{\log(\frac{f_f}{f_i})} \tag{2}$$

Given the physical characteristics of the bender actuator system, a nonlinear spring-mass-damper system was chosen as the

model structure. The spring component of the model corresponds to the elasticity of the silicone body of the bender. The inertial mass of the system is primarily represented in the mass of the fluid. The damping effects possibly originate from the non-linear viscoelastic properties of the elastomer.

The curves from the two static tests informed the selection of the nonlinear terms (x^3,x^2) and their derivatives in the model. This resulted in the model structure shown in Eqn. (3-5), where F is the bender force exerted on the distal tip, X are the model terms which correspond to the volume (x) and its derivatives Eqn. (4), and Φ are the model parameters Eqn. (5). The constant term was used to eliminate any pre-loading of the actuator on the load cell. A 'grey box' system identification process was then applied to the soft actuator data to solve for the model parameters, Φ [28]. Using non-negative least squares, the unknown parameters, Φ, were estimated as shown in Eqn. (6), where F_m is the force measured by the loadcell [29].

$$F = X\Phi \tag{3}$$

$$X = [\dot{x}^3 \quad \dot{x}^2 \quad \ddot{x} \quad \dot{x}^3 \quad \dot{x}^2 \quad \dot{x} \quad x^3 \quad x^2 \quad x \quad 1] \tag{4}$$

$$\Phi = [C_1 \quad ... \quad C_n]^T \tag{5}$$

$$\min_{\Phi} \|X\Phi - F_m\|_2^2 \quad where \quad \Phi > 0 \tag{6}$$

The contribution and relative importance of individual terms to the overall accuracy of the model was also investigated. A single term indexed by (p) was dropped from Eqn. (4) and the parameters were recomputed using Eqn. (6). The percent change in accuracy was subsequently recorded. The root mean squared error (RMSE) and the cumulative RMSE were evaluated using Eqn. (8) and Eqn. (9), respectively, and were used as a metric to evaluate the fit of the model. The difference of cumulative RMSE was found via Eqn. (10), where $\emptyset$ corresponds to a model with no model terms removed and p represents a model with the p-th term removed from the analysis, both as a function of time (t). Then the results of Eqn. (10) were plotted, and the variables with the most significant impact remained in the model. Conversely, variables that showed no perceptible difference in cumulative error when removed or added to the model were used to explore relative importance. For example, if a dynamic term indicated by a time derivative was important, it should indicate a significant change in cumulative error if removed from the least squares fit.

$$\tilde{F}(t) = F_m(t) - X(t)\Phi \tag{7}$$

$$RMSE = \Big(\sum_{i=t_i}^{t_f} \tilde{F}(t)^2\Big)^{0.5} \tag{8}$$

$$RMSE_{cum}(t) = \Big(\sum_{i=0}^{t} \tilde{F}(i)^2\Big)^{0.5} \tag{9}$$

$$RMSE_{diff}(t,p) = RMSE_{cum}(t,p) - RMSE_{cum}(t,\emptyset) \tag{10}$$

To establish the optimal model that maximizes efficiency while minimizing model complexity, relative reductions in RMSE were investigated. This was performed by increasing the number of model terms monotonically from 1 to 6 with all possible permutation of model terms in each increment and including constant term in each iteration. The minimum RMSE in each increment was computed in order to determine convergence in the model. A threshold of 1% decrease in total RMSE for increase in model term was adopted as a criteria for selecting the optimal model.

RESULTS

The output of the quasi-static ramp test shown in Figure 6 provides a static map of the contact force output of the bender as a function of the fluid volume input. An intuitive relationship is observed. With increased fluid volume in the actuator, the cavity pressure increases. This pressure results in a stronger bend that is translated into contact force at the actuator tip. This test also shows the constrained loading condition produces larger forces, as the roller joint directs more of the bending actuation into the load cell, producing larger contact forces at the distal tip.

The multi-level staircase response investigates energy storage of the soft actuator during the expansion and contraction stages of the cycle. Figure 7 shows how the energy, represented by the area within the curves, is stored throughout the actuation cycle.

The dynamic chirp signal was used to develop the system models and to understand the behavior of the soft actuator under different frequency inputs. The observed response of the dynamic chirp test is shown in Figure 8

Figure 9 & Figure 11 show the relative contribution of each term to the overall error for both loading conditions respectively. This indicates that the model terms representing dynamics (time derivatives) play a relatively minor role in the model individually.

The RMSE value for the unconstrained loading condition were plotted for all possible combinations of number of model terms in Figure 10. The minimum RMSE for each number of model terms were highlighted and used in a convergence criterion. The 1% convergence threshold resulted in three effective

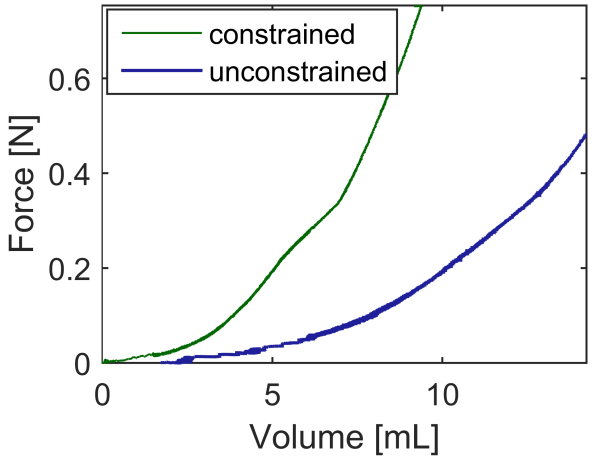

FIGURE 6: Quasi-static ramp response

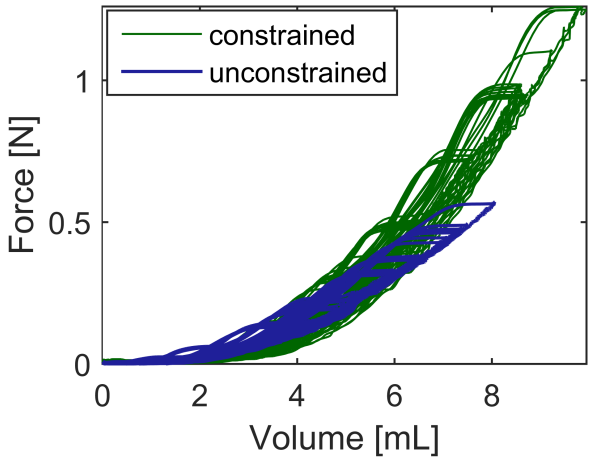

FIGURE 7: Multi-level staircase response

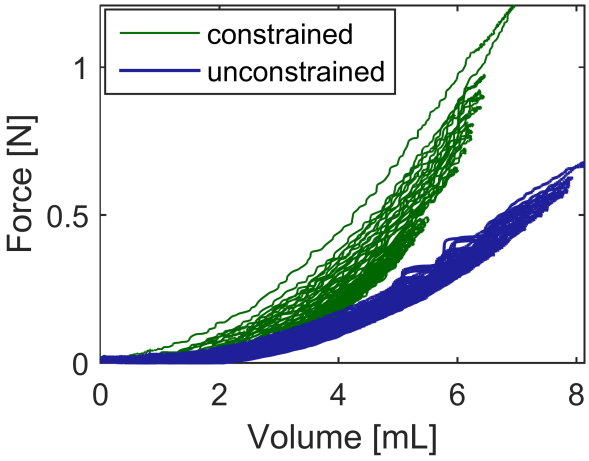

FIGURE 8: Dynamic chirp response

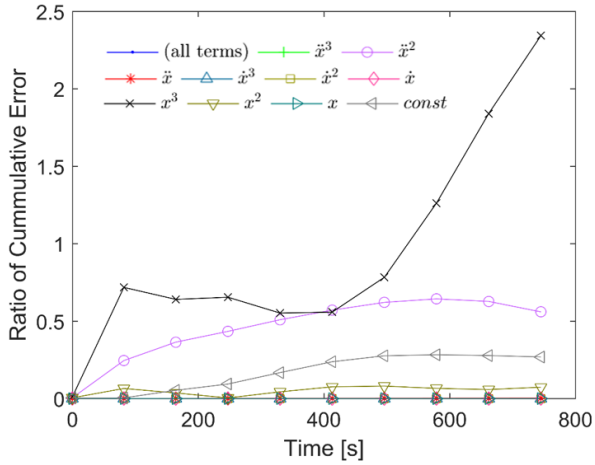

FIGURE 9: The cumulative RMSE difference of the unconstrained model, in respect to all terms, when a single parameter is dropped from the analysis.

model terms, which were used to build the optimized unconstrained model F_{unc} as shown in Eqn. (11).

$$F_{unc} = \begin{pmatrix} \ddot{x}^2 & x^3 & x^2 & 1 \end{pmatrix} \begin{pmatrix} 4.73 \times 10^{-7}[Nm^{-6}s^4] \\ 7.88 \times 10^{-4}[Nm^{-9}] \\ 3.47 \times 10^{-3}[Nm^{-6}] \\ 1.22 \times 10^{-2}[N] \end{pmatrix} \tag{11}$$

In the constrained loading conditions the RMSE method was applied to find the maximum number of model terms which influenced the force with a 1% convergence as shown in Figure 12. The minimum RMSE resulted in one effective model term x^3.

The simplified constrained system model for the force, (F_{con}), is shown in Eqn. (12).

$$F_{con} = \begin{pmatrix} x^3 & 1 \end{pmatrix} \begin{pmatrix} 6.52 \times 10^{-4}[Nm^{-9}] \\ 2.42 \times 10^{-3}[N] \end{pmatrix} \tag{12}$$

The reduced term models (F_{unc} and F_{con}) were compared to the experimental data in order to verify the accuracy of the model. Figure 13 indicates that the reduced models are consistent with the experimental results well.

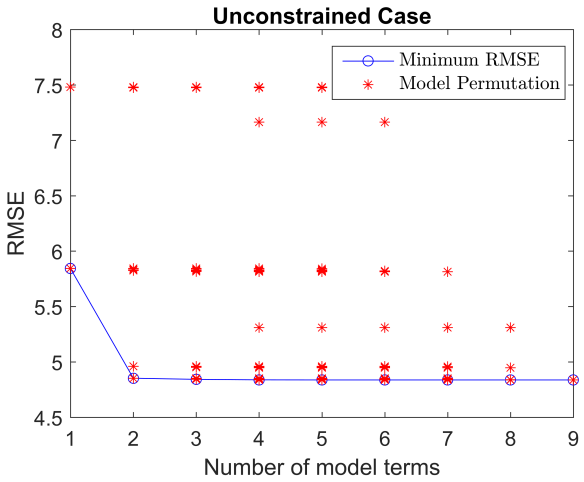

FIGURE 10: The RMSE values resulting from combination of different number of model terms for the unconstrained conditions

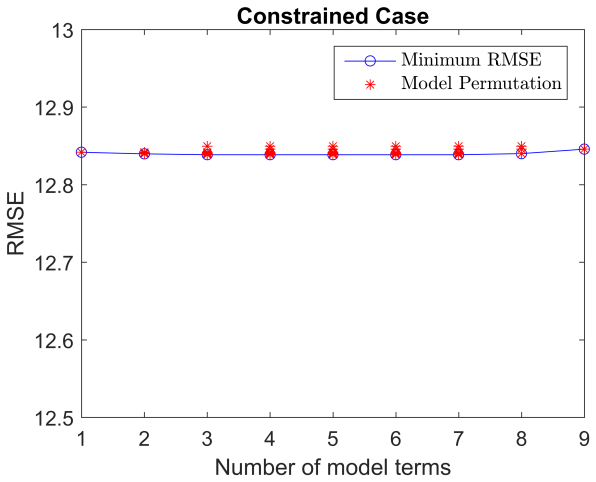

FIGURE 12: The RMSE values resulting from combination of different number of model terms for the constrained conditions

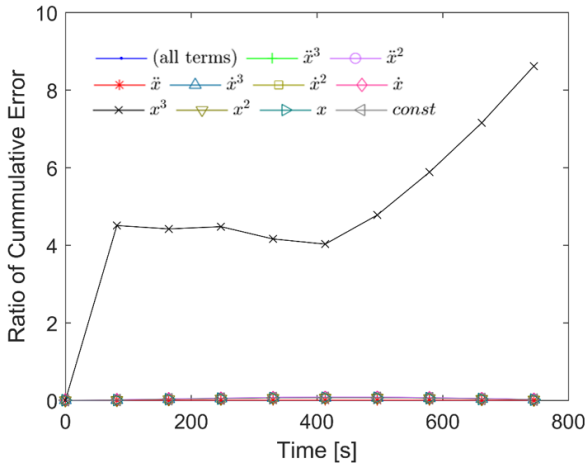

FIGURE 11: The cumulative RMSE difference of the constrained model, with respect to all terms, when a single parameter is dropped from the analysis.

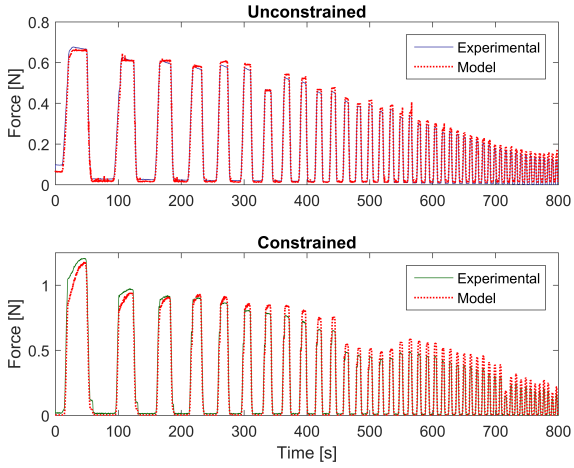

FIGURE 13: Model fit of the time data with respect to the force, left is the unconstrained model, right is the constrained model.

DISCUSSION

By analyzing the system identification data, important elements of future bender control in intravascular procedures can be identified. The static analysis shows that larger forces are generated when the bender is in the constrained loading configuration as opposed to the unconstrained configuration. Understanding the difference between these models will be an important component of planning soft catheter procedures in the future. Constrained loading conditions are more likely to appear in small diameter vasculature, while unconstrained conditions could appear during procedures within the chambers of the heart.

The hysteresis and dynamic relaxation of the silicone material have a large effect on the model. From the multi-level loading and unloading test results in Figure 7, we clearly see a large difference between the pressurization and depressurization curves. As with the loading conditions, this hysteresis effect may require a separate model for inflating and deflating the bender. The non-linear relaxation of the material can also be clearly seen in Figure 8. As the test progressed, the same volume input resulted in less contact force. These test results may also indicate that end effector sensing feedback may be the best way to provide accurate control of the soft actuator end effector in the context of an intravascular procedure.

Chirp signals were used to identify the system model. The original system has nine effective model terms and the contribution of each model term towards system output varies. The less influential model terms have been removed to develop a reduced system model for better analysis. In the unconstrained force model (F_{unc}) the model terms $\ddot{x}^3$, $\ddot{x}$, $\dot{x}^3$, $\dot{x}^2$, $\dot{x}$ and x were removed, while $\ddot{x}^3$, $\ddot{x}^2$, $\ddot{x}$, $\dot{x}^3$, $\dot{x}^2$, $\dot{x}$, x^2 and x were removed in the constrained force model (F_{con}). In these force models the distal tip of the actuator is in contact with the load cell, which may negate some damping effects from the inertial mass of the elastomer. This also accounts for the constant preload term in Equation 11 and 12. The two system models (F_{unc}) and (F_{con}) are not identical in form and vary significantly in different loading conditions. Notably, a dynamic term ($\ddot{x}^2$) appears in (F_{unc}) but not in (F_{con}). This may be due to the unconstrained case having a lower overall stiffness and thereby allowing a interial fluid forces to be more apparent. In either case, the reduced models (Eqn. 12 and 11) in concert with the observations of relative influence of individual variables (Fig. 10 and 12) indicate that dynamics play a negligible role in this actuators performance, particularly when compared to the nonlinear stiffness.

The inability of a single model to predict bender contact force for a variety of loading conditions will complicate attempts to control the soft actuator. This investigation suggests that the system will either need to select from a variety of models based on the loading configuration, or simply have accurate force sensing at the distal tip to incorporate successful control. Either way, robust and intravascular compatible sensing modalities will be required for force control applications within the surgical suite.

CONCLUSION

This work provides an initial investigation of the soft actuator output force system in order to evaluate the potential of soft actuators to serve as catheter robots. Intravascular diagnostics and therapy delivery are often sensitive to the degree of device contact force, therefore a soft catheter robot must have contact force control at the end effector. Static and dynamic system identification tests were performed on a bender actuator in two different loading conditions, and reduced models were successfully developed and empirically confirmed for the dynamic output contact force as a function of input volume.

The non-linearities of the soft actuator material presented hysteresis effects on the inflation and deflation cycle, as well as contributed to the stress relaxation of the bender over time. These characterizations will need to be addressed in the future control of the bender. It was also shown that the bender dynamics appeared to play a minimal role, especially compared to nonlinear stiffness.

The reduced models developed by the RMSE method closely matched the experimental results. The system models for the two different loading conditions varied in both the significant terms and the parameter values. From these results, it is inferred that modeling a more complete set of loading conditions will result in a wide number of different models. Therefore, to accurately predict the force output, the loading conditions must either be known or the system must have accurate contact force feedback.

Implementing force control is an important step for soft robotic catheter clinically relevancy. While the results from this work are encouraging, future work is needed to successfully apply force control on a soft bender actuator. Proper loading conditions need to be identified in order to select the most accurate model. Despite such challenges, soft actuators show potential to be used in soft catheter robot due to their inherent compliance and biocompatibility.

ACKNOWLEDGMENT

We would like to thank the MnDrive (Minnesota's Discovery, Research, and InnoVation Econonomy) initiative for financial support. We would also like to thank Dr. Arthur Erdman and the Medical Devices Center for supplying the necessary laboratory space and tools, as well as Dr. Robert Sweet, Troy Rheisen, and Jason Speich of the CREST (Center for Research in Education and Simulation Technologies) lab at the University of Minnesota Medical School for providing suggestions and resources for the silicone molding.

References

[1] , 2014. Faststats: Inpatient surgery, May.

[2] Popma, J., Almonacid, A., Burke, D., and Topol, E. J., 2012. *Textbook of interventional cardiology*. Elsevier.

[3] Cugmas, B., Bürmen, M., Bregar, M., Pernuš, F., and Likar, B., 2013. "Pressure-induced near infrared spectra response as a valuable source of information for soft tissue classification". *Journal of biomedical optics,* ***18***(4), pp. 047002–047002.

[4] Cugmas, B., Bregar, M., Bürmen, M., Pernuš, F., and Likar, B., 2014. "Impact of contact pressure–induced spectral changes on soft-tissue classification in diffuse reflectance spectroscopy: problems and solutions". *Journal of biomedical optics,* ***19***(3), pp. 037002–037002.

[5] Reddy, V. Y., Shah, D., Kautzner, J., Schmidt, B., Saoudi, N., Herrera, C., Jaïs, P., Hindricks, G., Peichl, P., Yulzari, A., et al., 2012. "The relationship between contact force and clinical outcome during radiofrequency catheter ablation of atrial fibrillation in the toccata study". *Heart Rhythm,* ***9***(11), pp. 1789–1795.

[6] Tilz, R. R., Makimoto, H., Lin, T., Rillig, A., Metzner, A., Mathew, S., Deiss, S., Wissner, E., Rausch, P., Kamioka, M., et al., 2014. "In vivo left-ventricular contact force analysis: comparison of antegrade transseptal with retrograde

transaortic mapping strategies and correlation of impedance and electrical amplitude with contact force". *Europace,* ***16***(9), pp. 1387–1395.

[7] Inderbitzi, R. G. C., Schmid, R. A., Melfi, F. M., and Casula, R. P., 2012. "Minimally invasive thoracic and cardiac surgery: Textbook and atlas".

[8] Andrikopoulos, G., Nikolakopoulos, G., and Manesis, S., 2011. "A survey on applications of pneumatic artificial muscles". In Control & Automation (MED), 2011 19th Mediterranean Conference on, IEEE, pp. 1439–1446.

[9] Chou, C.-P., and Hannaford, B., 1996. "Measurement and modeling of mckibben pneumatic artificial muscles". *Robotics and Automation, IEEE Transactions on,* ***12***(1), pp. 90–102.

[10] Tondu, B., 2012. "Modelling of the mckibben artificial muscle: A review". *Journal of Intelligent Material Systems and Structures,* ***23***(3), pp. 225–253.

[11] Bishop-Moser, J., and Kota, S., 2015. "Design and modeling of generalized fiber-reinforced pneumatic soft actuators". *Robotics, IEEE Transactions on,* ***31***(3), June, pp. 536–545.

[12] Bishop-Moser, J. L., 2014. "Design of generalized fiber-reinforced elasto-fluidic systems". PhD thesis, University of Michigan.

[13] Bishop-Moser, J., and Kota, S., 2013. "Towards snake-like soft robots: Design of fluidic fiber-reinforced elastomeric helical manipulators". In Intelligent Robots and Systems (IROS), 2013 IEEE/RSJ International Conference on, IEEE, pp. 5021–5026.

[14] Krishnan, G., 2014. "Kinematics of a new class of smart actuators for soft robots based on generalized pneumatic artificial muscles". In Intelligent Robots and Systems (IROS 2014), 2014 IEEE/RSJ International Conference on, IEEE, pp. 587–592.

[15] Krishnan, G., Bishop-Moser, J., Kim, C., and Kota, S., 2012. "Evaluating mobility behavior of fluid filled fiber-reinforced elastomeric enclosures". In ASME 2012 International Design Engineering Technical Conferences and Computers and Information in Engineering Conference, American Society of Mechanical Engineers, pp. 1089–1099.

[16] Bishop-Moser, J., Krishnan, G., and Kota, S., 2013. "Force and moment generation of fiber-reinforced pneumatic soft actuators". In Intelligent Robots and Systems (IROS), 2013 IEEE/RSJ International Conference on, IEEE, pp. 4460–4465.

[17] Bishop-Moser, J., Krishnan, G., and Kota, S., 2013. "Force and hydraulic displacement amplification of fiber reinforced soft actuators". In ASME 2013 International Design Engineering Technical Conferences and Computers and Information in Engineering Conference, American Society of Mechanical Engineers, pp. V06AT07A031–V06AT07A031.

[18] Galloway, K. C., Polygerinos, P., Walsh, C. J., and Wood, R. J., 2013. "Mechanically programmable bend radius for fiber-reinforced soft actuators". In Advanced Robotics (ICAR), 2013 16th International Conference on, IEEE, pp. 1–6.

[19] Maeder-York, P., Clites, T., Boggs, E., Neff, R., Polygerinos, P., Holland, D., Stirling, L., Galloway, K., Wee, C., and Walsh, C., 2014. "Biologically inspired soft robot for thumb rehabilitation". *Journal of Medical Devices,* ***8***(2), p. 020933.

[20] Polygerinos, P., Wang, Z., Overvelde, J. T., Galloway, K. C., Wood, R. J., Bertoldi, K., and Walsh, C. J., 2015. "Modeling of soft fiber-reinforced bending actuators".

[21] Sun, Y., Song, Y. S., and Paik, J., 2013. "Characterization of silicone rubber based soft pneumatic actuators". In Intelligent Robots and Systems (IROS), 2013 IEEE/RSJ International Conference on, Ieee, pp. 4446–4453.

[22] Beekman, D., Bijadi, S., and Kowalewski, T., 2014. "Real-time tissue differentiation using fiber optic sensing in laser catheters". *Journal of Medical Devices,* ***8***(3), p. 030934.

[23] Beekman, D., and Kowalewski, T., 2015. "Variable-contact diffuse reflectance spectroscopy in intravascular conditions assessment". *Journal of Medical Devices,* ***9***(3), p. 030940.

[24] Suri, V., Gupta, R., Sharma, G., and Suri, K., 2014. "An unusual cause of ischemic stroke-cerebral air embolism". *Annals of Indian Academy of Neurology,* ***17***(1), p. 89.

[25] Xia, J., and Durfee, W. K., 2011. "Modeling of tiny hydraulic cylinders". pp. 1–5.

[26] Galloway, K. C., and Polygerinos, P. Soft robotics toolkit.

[27] Novák, A., Simon, L., Kadlec, F., and Lotton, P., 2010. "Nonlinear system identification using exponential swept-sine signal". *Instrumentation and Measurement, IEEE Transactions on,* ***59***(8), pp. 2220–2229.

[28] Sjöberg, J., Zhang, Q., Ljung, L., Benveniste, A., Delyon, B., Glorennec, P.-Y., Hjalmarsson, H., and Juditsky, A., 1995. "Nonlinear black-box modeling in system identification: a unified overview". *Automatica,* ***31***(12), pp. 1691–1724.

[29] Lawson, C. L., and Hanson, R. J., 1974. *Solving least squares problems*, Vol. 161. SIAM.